*Journal of Engineering Mathematics* **41:** 345–366, 2001.


# Nonlocal problems in MEMS device control

J.A. PELESKO[1] and A.A. TRIOLO[2]
[1]*Georgia Institute of Technology, Atlanta, GA 30332-0160, U.S.A. (e-mail: pelesko@math.gatech.edu)*
[2]*Lucent Technologies, Whippany, NJ, U.S.A. (e-mail: atriolo@lucent.com)*

Received 25 February 2000; accepted in revised form 29 May 2001

**Abstract.** Perhaps the most ubiquitous phenomena associated with electrostatically actuated MEMS devices is the 'pull-in' voltage instability. In this instability, when applied voltages are increased beyond a certain critical voltage there is no longer a steady-state configuration of the device where mechanical members remain separate. This instability severely restricts the range of stable operation of many devices. Here, a mathematical model of an idealized electrostatically actuated MEMS device is constructed for the purpose of analyzing various schemes proposed for the control of the pull-in instability. This embedding of a device into a control circuit gives rise to a nonlinear and *nonlocal* elliptic problem which is analyzed through a variety of asymptotic, analytical, and numerical techniques. The pull-in voltage instability is characterized in terms of the bifurcation diagram for the mathematical model. Variations in various capacitive control schemes are shown to give rise to variations in the bifurcation diagram and hence to effect the pull-in voltage and pull-in distance.

**Key words:** MEMS, microelectromechanical systems, nonlocal elliptic problem

## 1. Introduction

The field of microelectromechanical systems (MEMS) has undergone a startling revolution in recent years. It is now possible to produce functioning motors that can only be seen with the aid of a microscope, gears smaller than a grain of pollen, and needles so tiny they can deliver an injection without stimulating nerve cells. The use of existing integrated circuit technology in the design and production of MEMS devices allows these devices to be batch-processed, hence made in quantity, inexpensively. This in turn is igniting a revolution in areas such as biotechnology, where devices that once could only be dreamed about have suddenly been made possible.

The ability to manufacture mechanical parts such as gears and levers on a length scale characterized by microns is not however the end of the story. The challenge is also to understand how physical systems behave on these scales. That is, an understanding of fluid, electromagnetic, thermal, and mechanical forces on the micron length scale is necessary in order to understand the operation and function of MEMS devices.

Applied forces used to provide locomotion for MEMS devices are of particular interest. It is neither feasible nor desirable to attempt to reproduce modes of locomotion that work on a macroscopic scale. For example, magnetic forces, which are often used for actuation in the macro world, scale poorly into the micro domain decreasing in strength by a factor of ten thousand when linear dimensions are reduced by a factor of ten [1]. This unfavorable scaling renders magnetic forces essentially useless. At the micron level, researchers have proposed a variety of new modes of locomotion based upon thermal, biological, and electrostatic forces. Each of these forces scales favorably as the linear dimensions of the system are decreased.

The canonical example, and the subject of this paper, is the utilization of electrostatic forces for MEMS device actuation. In general [1], electrostatic forces only decrease by a factor of one hundred when linear dimensions decrease by a factor of ten. With a slight increase in electric field strength, it is even possible to obtain a one to one scaling between force and linear dimension.

This highly favorable scaling was recognized and exploited as early as 1967 by Nathanson *et al.* [2]. In their seminal paper, Nathanson and his coworkers describe the manufacture, experimentation with, and modeling of a millimeter sized resonant gate transistor. This early MEMS device utilized both electrical and mechanical parts on the same substrate. Numerous benefits of such an approach, including size savings, cost savings, and improved efficiency were demonstrated. However, even at this early stage of MEMS research, the ubiquitous 'pull-in' voltage instability was encountered. In this instability, when applied voltages are increased beyond a certain critical voltage, there is no longer a steady-state configuration of the device where mechanical members remain separate. That is, device components crash together and often stick or break leading to device failure. This instability severely restricts the range of stable operation of many devices.

Recently, several authors have proposed and analyzed control schemes in an effort to overcome this instability. Chu and Pister [3], proposed a voltage control algorithm, while Seeger and Crary [4, 5], and Chan and Dutton [6], studied capacitive control schemes. In this paper we focus on control via the addition of a series capacitance. In [4], Seeger and Crary analyzed a control scheme which placed a fixed capacitor in series with a MEMS device by studying a mass-spring model. In the course of their analysis, nonlinear terms arising from the electrostatic force and from the additional capacitance were found to cancel. This led to the result that the scheme could stabilize a device over the entire range of motion. In [6], 2-D effects were included in a mass-spring model in an ad-hoc manner. In particular they modeled the force on an electrostatically actuated 2-D beam through a lumped element representation. Essentially, the beam was chopped into two pieces with different deflections to capture the difference in behavior between the edges and the center. This was then treated as two parallel plate MEMS devices placed in series. Mathematically, this removed the cancellation of nonlinear terms seen by Seeger and Crary and led to the conjecture that the control scheme is only partially stabilizing. In [5] an MOS capacitor was used in place of the fixed capacitor. When run in deep depletion, the MOS device acts a varactor. That is, the capacitance of the device is now voltage-dependent. Seeger and Crary showed that this scheme led to greater stabilization with a lower energy cost. Again, their analysis was done with the aid of a mass-spring model.

In this paper, we analyze both series capacitance control schemes in the context of a two dimensional model. In particular, we model the device shown in Figure 1, which consists of an elastic strip suspended above a rigid plate. The strip is held fixed at two ends and remains unsupported along the other edges. This structure is a common MEMS building block. It is easy to fabricate using a variety of materials and is particularly versatile. Examples of the fabrication and use of this structure appear in references [7–9]. In this paper we treat the strip as an elastic membrane. While this approximation will not be valid for all MEMS devices, it will be valid for many, such as micropumps made of thin glassy polymers [10, 11] or devices such as the grating light valve (GLV), composed of thin ribbons held under tension [12]. Also it will be a good approximation for devices whose thickness is many times less than their deflection, [13, pp. 344–345], such as those discussed in [3, 14–18]. Further, even for devices for which bending stresses cannot be ignored, we expect our model to yield qualitative if not quantitative understanding. Next, the device is embedded in a simple closed circuit

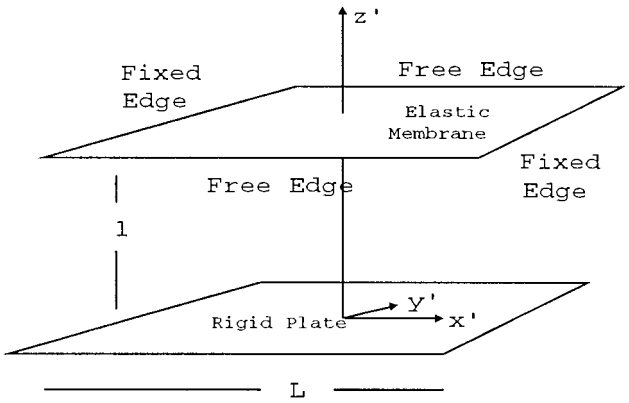


*Figure 1.* Geometry of our idealized MEMS device.

consisting of a battery and either a fixed capacitor or a varactor. The model consists of the circuit equations, the equation of elasticity for the strip, and the potential equation for the electrostatic field. We assume that the device has a small aspect ratio and use an asymptotic method to obtain an approximate solution to the potential equation. The same method is used to compute an approximation to the capacitance of our idealized device. The validity of these approximations is verified by comparison with numerical solutions of the potential equation. Using the approximate solutions for the potential in the equation of elasticity, we obtain a nonlinear and *nonlocal* differential equation for the shape of the deflected membrane. We analyze this equation using a combination of asymptotic, rigorous analytical, and numerical techniques. We relate the nonlocal problem to a local problem through a simple mapping. The local problem was partially analyzed in [19]. We utilize the mapping between the local and nonlocal problems to translate several of the results in [19] to results about the nonlocal problem. Next, utilizing the symmetry of the local problem, we characterize the bifurcation diagram for the mathematical model and the pull-in instability in terms of this bifurcation diagram. In particular, we verify the conjecture of Chan and Dutton that 2-D effects limit the success of the fixed capacitive control scheme, *i.e.* the pull-in instability persists. We show how variations in the capacitance of the fixed capacitor effect the pull-in voltage and pull-in distance. The mathematical model for the varactor control scheme is algebraically more complicated. Nevertheless, we are able to use tools similar to those employed for the fixed scheme in order to gain an understanding of the behavior of solutions for this model. Once again, the bifurcation diagram is sketched and used to show how the control scheme effects the pull-in instability. In particular, we show that the varactor also exerts a stabilizing influence on the system, but at a lower voltage cost than the fixed capacitor.

## 2. Formulation of the model

In this section we present the governing equations for the behavior of an idealized electrostatically actuated MEMS device. We begin with the equations which govern the electrostatic field, and hence the electrostatic forces on device components. In doing so, we find that the specification of the electrostatic potential for our model requires that we prescribe the voltage drop across the device. In turn, this voltage drop depends upon other circuit components and

the current device configuration. In a pair of subsections, we compute the voltage drop across our device for two proposed control circuits.

Our idealized device consists of an elastic membrane suspended above a rigid plate. Both membrane and plate have width $w$, length $L$ and are separated by a gap of height $l$. The geometry is sketched in Figure 1. A potential difference is applied between the membrane and the plate, which are both assumed to be perfect conductors. With these assumptions in mind, we formulate the equations governing the electrostatic potential in the region surrounding the device, and the elastic displacement of the membrane. The electrostatic potential, $\phi$, satisfies

$$\nabla^2\phi = 0, \tag{1}$$

$$\phi(x', y', -l) = 0, \quad x' \in [-L/2, L/2], \quad y' \in [-w/2, w/2], \tag{2}$$

$$\phi(x', y', u') = V_s f(u'/l), \quad x' \in [-L/2, L/2], \quad y' \in [-w/2, w/2], \tag{3}$$

where here $u'(x')$ is the displacement from $z' = 0$ of the membrane, $V_s$ is the source voltage and the function $f$ embodies the fact that the voltage drop across our device when embedded in a circuit may depend upon $u'$. Note that $f$ is a dimensionless function. Further note that we are assuming a one-dimensional nature to the displacement, *i.e.* $u'$ is a function of $x'$ only. In general, we expect the displacement to be a function of both $x'$ and $y'$. However, to clarify the role of 2-D effects on capacitive control schemes, the assumption that $u'$ is a function of $x'$ alone is sufficient. Of course, this leads to simplification in the analysis which follows. This displacement is assumed to satisfy a one dimensional membrane equation

$$T\frac{\mathrm{d}^2u'}{\mathrm{d}x'^2} = \frac{\epsilon_0}{2}|\nabla\phi|^2 \tag{4}$$

with right-hand side proportional to the norm of the gradient of the electrostatic potential. Here, $T$ is tension and $\epsilon_0$ is the permittivity of free space. We assume that the membrane is held fixed along the edges at $x = \pm L/2$ and impose the boundary conditions

$$u'(-L/2) = u'(L/2) = 0. \tag{5}$$

Implicit in the assumption that $u'$ is a function of $x'$ alone is the assumption that the remaining edges are free.

Next, we introduce dimensionless variables and rewrite our governing equations in dimensionless form. We define

$$\psi = \phi/V_s, \quad u = u'/l, \quad x = x'/L, \quad y = y'/w, \quad z = z'/l \tag{6}$$

and substitute these in Equations (1)–(5). This yields

$$\epsilon^2\left(\frac{\partial^2\psi}{\partial x^2} + a^2\frac{\partial^2\psi}{\partial y^2}\right) + \frac{\partial^2\psi}{\partial z^2} = 0, \tag{7}$$

$$\psi(x, y, -1) = 0, \quad x \in [-1/2, 1/2], \quad y \in [-1/2, 1/2], \tag{8}$$

$$\psi(x, y, u) = f(u), \quad x \in [-1/2, 1/2], \quad y \in [-1/2, 1/2], \tag{9}$$

$$\frac{\mathrm{d}^2u}{\mathrm{d}x^2} = \beta\left(\epsilon^2\left(\frac{\partial\psi}{\partial x}\right)^2 + \epsilon^2a^2\left(\frac{\partial\psi}{\partial y}\right)^2 + \left(\frac{\partial\psi}{\partial z}\right)^2\right), \tag{10}$$

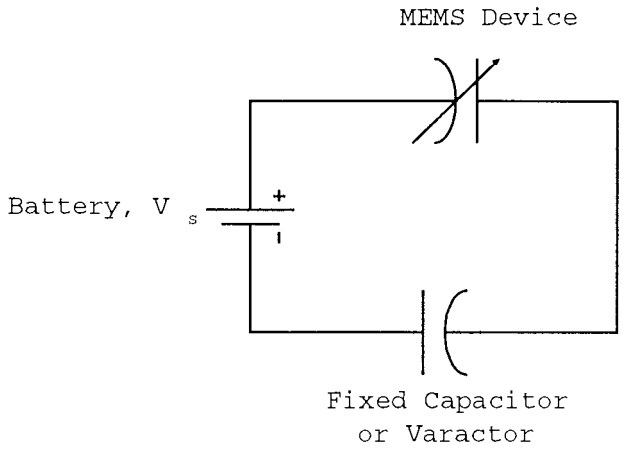


*Figure 2.* Sketch of the basic control circuit.

$$u(-1/2) = u(1/2) = 0. \tag{11}$$

Here $\epsilon = l/L$ is an aspect ratio comparing device length to gap size, $a = L/w$ is an aspect ratio of the device itself and $\beta = \epsilon_0 V_s^2 L^2/2Tl^3$ is a dimensionless number which characterizes the relative strengths of electrostatic and mechanical forces in the system.

### 2.1. Fixed capacitive control

As previously mentioned when our device is embedded in a circuit, the voltage drop across the device, $V$, depends upon other circuit elements and the current device configuration. By applying Kirchoff's laws, we find that the voltage drop, $V$, across our idealized MEMS device is given by

$$V = \frac{V_s}{1 + C/C_f} \tag{12}$$

when the device is embedded in the circuit shown in Figure 2. This is the control scheme proposed in [4] and studied using mass-spring models in [4, 6]. Note that the only additional component is a fixed capacitor. This means that the circuit acts as a voltage divider and exerts a stabilizing influence on the device. That is, our device is itself a capacitor, and its capacitance, $C$, appearing in Equation (12), is a function of device position. This capacitance will increase as the membrane approaches the rigid plate, causing $V$ to drop and hence reducing the electrostatic force, thereby stabilizing the device. Note that Equation (12) may be used to define $f$ for this circuit as

$$f(u) = \frac{1}{1 + C/C_f}. \tag{13}$$

In Section 3 we will present an approximate technique for computing the capacitance, $C$.

### 2.2. Varactor capacitive control

Again, we consider the circuit shown in Figure 2, with the modification that the previously fixed capacitor, $C_f$, is now taken to be a varactor. A special case of this setup was studied by

Seeger and Crary [5], using a mass-spring model. The result of substituting a varactor is that the capacitance, $C_f$, is now a function of the voltage drop across this varactor. If $V_f$ is this voltage drop, then the behavior of $C_f$ may be assumed to follow the power law

$$C_f = C_m(\frac{1}{1 - V_f/V_0})^{1/2}. \tag{14}$$

Here, $V_0$ is the contact junction potential and $C_m$ is the capacitance at zero applied voltage. We note that both parameters depend upon doping profiles and device geometry. The reader is referred to [20] for a full discussion of varactor models and varactor uses.

Now, as in the previous subsection, we may apply Kirchoff's laws and conclude that the voltage drop across our MEMS device, $V$, is given by

$$V = \frac{V_s}{1 + C/C_f}, \tag{15}$$

while $V_f$ is given by

$$V_f = -V - V_s. \tag{16}$$

Note that Equation (15) may be used to define $f$ for this device as

$$f(u) = \frac{1}{1 + C/C_f}, \tag{17}$$

where $C_f = C_f(u)$ is defined implicitly through

$$1 + \frac{V_s}{V_0}\left(\frac{2 + C/C_f}{1 + C/C_f}\right) - \left(\frac{C_m}{C_f}\right)^2 = 0. \tag{18}$$

Also, as in the previous subsection, the capacitance of our MEMS device, $C$, is unknown. In Section 3 we will present an approximate method for computing $C$ in terms of $u$.

## 3. The electrostatic field

In this section we explore techniques for obtaining approximate analytical and numerical solutions to the electrostatic problem, Equations (1)–(3). As we have seen, these solutions are necessary for computing both elastic forces on our device and the capacitance of our device. The problem of computing the electrostatic field, either asymptotically or numerically, for the purpose of figuring capacitance's and forces is an old problem with a rich history. The reader is directed to references [21] and [22] for a first look at this field. In this paper, our goals for these problems are two-fold. First, we wish to compute a simple approximate expression for the potential. This will allow us to reduce the problem to a nonlinear elliptic equation governing the elastic displacement. Second, we wish to verify that for the displacements thus obtained, our approximate potential is valid. The first goal is accomplished via a perturbation expansion, while the second is handled numerically.

### 3.1. AN ASYMPTOTIC THEORY

To compute the potential, we must solve

$$\epsilon^2\left(\frac{\partial^2\psi}{\partial x^2}+a^2\frac{\partial^2\psi}{\partial y^2}\right)+\frac{\partial^2\psi}{\partial z^2}=0, \tag{19}$$

$$\psi(x,y,-1)=0, \quad x\in[-1/2,1/2], \quad y\in[-1/2,1/2], \tag{20}$$

$$\psi(x,y,u)=f(u), \quad x\in[-1/2,1/2], \quad y\in[-1/2,1/2]. \tag{21}$$

To compute the capacitance of the device, we need the potential for the case $f(u)=1$ and then may compute the capacitance, $C$, through

$$C=C_0\int_{-1/2}^{1/2}\int_{-1/2}^{1/2}\frac{\partial\psi}{\partial z}(x,y,0)\,\mathrm{d}x\,\mathrm{d}y. \tag{22}$$

Note that $C_0$ is the capacitance of the undeflected device.

Here, we develop a leading-order theory by utilizing the fact that for a typical MEMS device the aspect ratio, $\epsilon$, is small. We assume that $a^2=O(1)$. Hence, we ignore terms of order epsilon squared in Equation (19). Then solving the resulting equation for the potential we easily find that

$$\psi=\frac{f(u)(1+z)}{1+u}. \tag{23}$$

Utilizing this approximation in our expression for the capacitance, we find that the normalized capacitance may be expressed as a functional of $u$ through

$$\frac{C}{C_0}=\int_{-1/2}^{1/2}\frac{\mathrm{d}\zeta}{1+u(\zeta)}. \tag{24}$$

### 3.2. NUMERICAL COMPARISON

In order to validate the aforementioned asymptotic solution, a 3-D moment method solution was constructed for the geometry shown in Figure 1, where the top plate is held at a normalized potential of one and the bottom plate is held at potential zero. The moment method analysis used here follows that of Harrington, [22, pp. 114–118], for the parallel plate capacitor, except in this case the top plate is deformed. The method is outlined here for convenience. The well-known solution to the electrostatic problem of a potential from an arbitrary charge distribution is

$$\psi(x,y,z)=\int\int\int\frac{\sigma(x',y',z')}{4\pi\epsilon R}\mathrm{d}x'\mathrm{d}y'\mathrm{d}z', \tag{25}$$

where $R=\sqrt{(x-x')^2+(y-y')^2+(z-z')^2}$ is the distance from the source point $(x',y',z')$ to the observation point $(x,y,z)$. For the geometry shown in Figure 1, the potential is specified as constant on two perfectly conducting, infinitely thin plates and the unknown charge densities on each of these plates is specified as $\sigma_t$ for the top plate and $\sigma_b$ for the bottom plate.

The boundary conditions on the top and bottom plates are $\psi = 1$, and $\psi = 0$, respectively. This results in the pair of coupled integral equations

$$1 = \int_{-1/2}^{1/2} dx' \int_{-1/2}^{1/2} dy' \left[ \frac{\sigma_t(x', y')}{4\pi\epsilon\sqrt{(x-x')^2 + (y-y')^2 + (u(x) - u(x'))^2}} + \frac{\sigma_b(x', y')}{4\pi\epsilon\sqrt{(x-x')^2 + (y-y')^2 + (u(x) + 1)^2}} \right], \tag{26}$$

$$0 = \int_{-1/2}^{1/2} dx' \int_{-1/2}^{1/2} dy' \left[ \frac{\sigma_t(x', y')}{4\pi\epsilon\sqrt{(x-x')^2 + (y-y')^2 + (1 + u(x'))^2}} + \frac{\sigma_b(x', y')}{4\pi\epsilon\sqrt{(x-x')^2 + (y-y')^2}} \right]. \tag{27}$$

The unknown charge densities can be found by breaking each plate into $N$ small subsections $\Delta s_n$ where the charge density can be considered constant. If we define basis functions

$$f_n = \begin{cases} 1 & \text{on} \Delta s_n \\ 0 & \text{on all other} \Delta s_m \end{cases}, \tag{28}$$

the two charge densities can be represented by

$$\sigma_t(x, y) \approx \sum_{n=1}^{N} \alpha_n f_n, \quad \sigma_b(x, y) \approx \sum_{n=N+1}^{2N} \alpha_n f_n. \tag{29}$$

The two integral equations now become summations, *i.e.*,

$$1 \approx \sum_{n=1}^{N} l_{mn}^{tt} \alpha_n + \sum_{n=N+1}^{2N} l_{mn}^{tb} \alpha_n, \tag{30}$$

$$0 \approx \sum_{n=1}^{N} l_{mn}^{bt} \alpha_n + \sum_{n=N+1}^{2N} l_{mn}^{bb} \alpha_n. \tag{31}$$

This system can be easily written in matrix form as

$$[l][\alpha_n] = [g_n], \tag{32}$$

where $[l]$ is a $2N$ x $2N$ matrix composed of submatrices as shown

$$[l] = \begin{bmatrix} [l^{tt}] & [l^{tb}] \\ [l^{bt}] & [l^{bb}] \end{bmatrix}. \tag{33}$$

The vector $[g_n]$ represents the boundary conditions on the potential, and in this case is written as

$$[g_n] = \begin{bmatrix} 1 \\ 1 \\ \vdots \\ 0 \\ 0 \\ \vdots \end{bmatrix}. \tag{34}$$

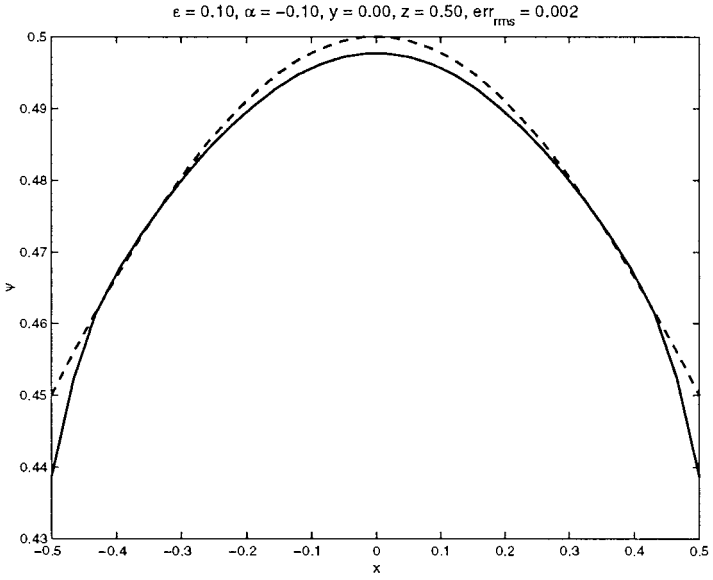


*Figure 3.* Comparison of potential half-way between the maximum deflection point on the deformed top plate and the flat bottom plate. The asymptotic approximation is dashed, the numerical solution solid. $\epsilon = 0{\cdot}1$, maximum deflection is $u = -0{\cdot}1$, r.m.s. error is 0·2%.

The integrals contained in $[l]$ must still be evaluated in order to solve this system. A point charge approximation is used in order to speed computation. This approximation assumes that the charge density on each subsection can be represented by a point charge and the potentials are evaluated at the centers of each subsection. The point charge approximation yields a 3·8% error for adjacent subsections and less for non-adjacent ones, [23].

Simulations were performed by use of the above method of moments (MoM) formulation for plate deformations governed by Equation (47). The two plates were each subdivided into 900 segments (30×30), the plate charge densities were found and subsequently used to find the potential as a function of $x$ halfway between the maximum deflection point and the bottom plate.

In order to evaluate the validity of the asymptotic (approximate) solution, we can define an rms error as

$$err_{rms} = \sqrt{\int_{-L/2}^{L/2} |\psi_{\text{asymptotic}} - \psi_{MoM}|^2 \mathrm{d}x}, \tag{35}$$

where $L$ is the length of the plate in the $x$-direction. R.m.s. errors for various values of maximum plate deflection $\alpha$ and ratios of plate separation to plate width $\epsilon$ are shown in Table 1. The ratio $\epsilon$ is varied by fixing the plate separation $l$ and changing the plate width in the $x$ direction ($L$). The observation point $z$ can be expressed as the fraction of the distance from the maximum deflection point $z = -\alpha$ to the fixed bottom plate at $z = -1$ by the following equation

$$z = -\alpha(1 - r) - r. \tag{36}$$

When $r = 0$, the observation point is located on the top plate at $y = 0$, $z = -\alpha$. When $r = 1$, the observation point is located on the bottom plate at $y = 0$, $z = -1$. Three cases

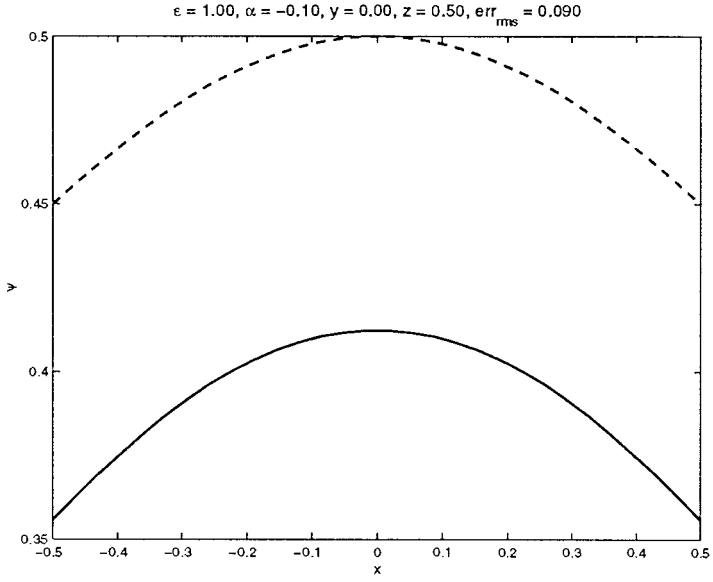


*Figure 4.* Comparison of potential half-way between the maximum deflection point on the deformed top plate and the flat bottom plate. The asymptotic approximation is dashed, the numerical solution solid. $\epsilon = 1$, maximum deflection is $u = -0{\cdot}1$, r.m.s. error is 9%.

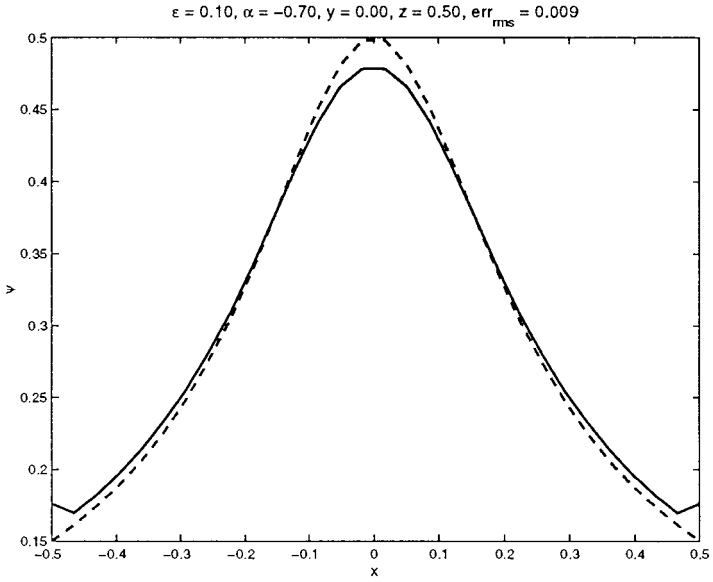


*Figure 5.* Comparison of potential half-way between the maximum deflection point on the deformed top plate and the flat bottom plate. The asymptotic approximation is dashed, the numerical solution solid. $\epsilon = 0.1$, maximum deflection is $u = -0{\cdot}7$, RMS error is 0.9%.

*Table 1.* Root mean square error in the asymptotic approximation for different values of the aspect ratio, maximum deflection and measurement point.

| $\epsilon$ | $\alpha$ | R.m.s. % at 1/4 | R.m.s. % at 1/2 | R.m.s. % at 3/4 |
|---|---|---|---|---|
| 0·1 | 0·7 | 2·2 | 0·9 | 0·4 |
| 0·25 | 0·7 | 3·5 | 2·4 | 0·5 |
| 0·75 | 0·7 | 7·4 | 5·6 | 2·8 |
| 1 | 0·7 | 8·7 | 6·7 | 4·4 |
| 0·1 | 0·1 | 0·4 | 0·2 | 0·4 |
| 0·25 | 0·1 | 1·1 | 0·8 | 1·2 |
| 0·75 | 0·1 | 6·3 | 5·7 | 3·1 |
| 1 | 0·1 | 9·9 | 9 | 3·8 |

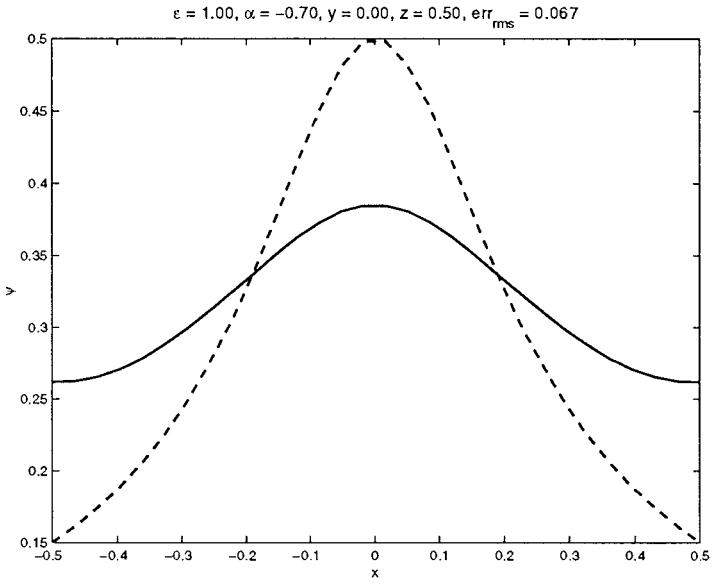


*Figure 6.* Comparison of potential half-way between the maximum deflection point on the deformed top plate and the flat bottom plate. The asymptotic approximation is dashed, the numerical solution solid. $\epsilon = 1$, maximum deflection is $u = -0{\cdot}7$, RMS error is 6.7%.

of observation point location were chosen to demonstrate $z$ dependence of the potential. One point is taken close to the maximum deflection point on the top plate ($r = 1/4$), the second point is midway between the maximum deflection point and the bottom plate ($r = 1/2$), the last is taken close to the bottom plate ($r = 3/4$).

Table 1 shows that the asymptotic solution is best when $\epsilon$ is small, that is, when the plate width is much larger than the plate separation. For $\epsilon = 0{\cdot}1$, the RMS error is less than 1% for both large deflections ($\alpha = 0{\cdot}7$) and small deflections ($\alpha = 0{\cdot}1$). The case where plate separation is equal to the plate width, $\epsilon = 1$, has r.m.s. errors less than 10% for all observation points. Representative data for two values each of $\alpha$ and $\epsilon$ are shown in Figures 3–6.

The asymptotic solution introduced in the previous section relies upon the assumption that fringing fields can be neglected when the plate separation is small compared to the plate width. This is quantitatively verified through the above numerical comparison, which shows a less than 1% r.m.s. error with small $\epsilon$. The numerical comparison also shows that even for resonably large $\epsilon$, the asymptotic solution is in error by less than 10%.

## 4. Analysis of fixed capacitive control

In this section we bring together our circuit analysis, approximate potential, and approximate capacitance calculations in order to derive a simple model of the elastic behavior of our MEMS device embedded in the capacitive control circuit, Figure 2.

First, making the small aspect ratio approximation, as was done in our field calculations, we may reduce our elastic model to

$$\frac{\mathrm{d}^2 u}{\mathrm{d}x^2} = \beta \left( \frac{\partial \psi}{\partial z} \right)^2, \tag{37}$$

$$u(-1/2) = u(1/2) = 0. \tag{38}$$

Now, recall from Section 3.1 that our approximate potential is given by

$$\psi = \frac{f(u)(1+z)}{1+u}, \tag{39}$$

while from Section 2.1 $f(u)$ is given by

$$f(u) = \frac{1}{1 + C/C_f}. \tag{40}$$

The approximate normalized capacitance was given in Section 3.1 as

$$\frac{C}{C_0} = \int_{-1/2}^{1/2} \frac{\mathrm{d}\zeta}{1+u(\zeta)} \tag{41}$$

and hence $f(u)$ may be rewritten as

$$f(u) = \frac{1}{1 + \chi \int_{-1/2}^{1/2} \frac{\mathrm{d}\zeta}{1+u(\zeta)}}, \tag{42}$$

where $\chi = C_0/C_f$. Now using this expression for $f$ together with Equation (39) in Equation (37), we obtain

$$\frac{\mathrm{d}^2 u}{\mathrm{d}x^2} = \frac{\beta}{(1+u)^2 (1 + \chi \int_{-1/2}^{1/2} \frac{\mathrm{d}\zeta}{1+u(\zeta)})^2} \tag{43}$$

as the governing equation for the elastic displacement of the membrane when the device is embedded in the simple capacitive control circuit, Figure 2. The boundary conditions remain unchanged, *i.e.*,

$$u(-1/2) = u(1/2) = 0. \tag{44}$$

Throughout the remainder of this section we shall analyze the solutions of Equations (43)–(44) in order to understand the circuits influence on our MEMS device. In particular, we are seeking solutions with $u > -1$ as $u \leq -1$ implies that the membrane and plate have collided.

We begin with the observation that Equations (43)–(44) are *nonlocal*. It is interesting to note that similar nonlocal equations arise in the study of Ohmic heating, again due to the influence of an electric field, see [24–26]. If we confine our attention to symmetric solutions a few elementary properties of solutions to Equations (43)–(44) follow almost by inspection. Since the second derivative is everywhere positive for positive $\beta$, the solution must be concave up everywhere or more succinctly, convex. Combining convexity with symmetry implies that $u(x) \geq u(0)$ for all $x \in [-1/2, 1/2]$. Finally, since the solution must be zero on the boundaries, and remain convex, we have that $u(x) \leq 0$ for all $x \in [-1/2, 1/2]$ as well. We summarize these results in the following theorem.

THEOREM 4.1. *Any smooth symmetric solution $u \in C^2[-1/2, 1/2]$ to Equations (43)–(44) satisfies*

*(i) $u$ is convex,*
*(ii) $u(x) \leq 0$ for all $x \in [-1/2, 1/2]$.*
*(iii) $u(x) \geq u(0)$ for all $x \in [-1/2, 1/2]$.*

In order to obtain a more detailed understanding of this nonlocal problem, which we shall denote (NLP), we will need to understand the nature of solutions for the associated local problem denoted (LP) which we define through the equations

$$\frac{\mathrm{d}^2 u}{\mathrm{d}x^2} = \frac{\lambda}{(1+u)^2}, \tag{45}$$

$$u(-1/2) = u(1/2) = 0. \tag{46}$$

We note that this system of equations governs the deflection of the membrane when the only other circuit element is a fixed voltage source. This may be seen as the problem (LP) results from setting $\chi = 0$ in (NLP). The relationship between solutions of problem (NLP) and problem (LP) is captured by the following key lemma.

LEMMA 4.1. *A solution, $u$, of problem (NLP) is a solution of problem (LP) for* $\lambda = \dfrac{\beta}{(1+\chi\int_{-1/2}^{1/2}\frac{\mathrm{d}\zeta}{1+u(\zeta)})^2}$, *while a solution, $u$, of problem (LP) is a solution of problem (NLP) for* $\beta = \lambda(1+\chi\displaystyle\int_{-1/2}^{1/2}\frac{\mathrm{d}\zeta}{1+u(\zeta)})^2$.

**Proof**. Obvious.

Note that this lemma implies that the set of solutions to (LP) and (NLP) are identical. Hence results concerning (LP) may be translated into results for (NLP), the translation being through the mapping between $\beta$ and $\lambda$ given in the lemma. Throughout the remainder of this section we shall restrict our attention to positive values of $\lambda$ and $\beta$, as this is the physical regime. We further note that (LP) was partially analyzed in [19] and in fact Theorem 4.1 could have be proved by comparison with (LP) together with Lemma 4.1.

An easy first example of the translation of results is the existence of a bound from below on smooth solutions to (NLP).

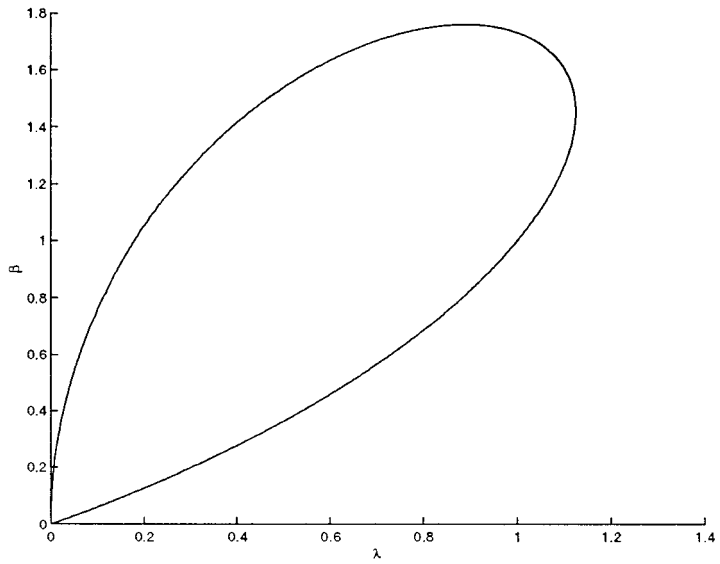


*Figure 7.* Sketch of the λ versus β curve.

THEOREM 4.2. *Any smooth symmetric solution, $u \in C^2[-1/2, 1/2]$, is bounded from below by $-1$. That is $u$ satisfies*

*(i)* $0 \geq u(x) \geq u(0) > -1$

**Proof**. The inequality holds true for (LP) as discussed in [19], to obtain for (NLP) apply Lemma 4.1.

As a second example of the translation of results we formulate a local existence theorem. For problem (LP) we have

THEOREM 4.3. *For any $\epsilon > 0$ there exists a $\lambda(\epsilon) > 0$ such that a unique solution to problem (LP) may be found in the set*

$$S_\epsilon = \{u(x) \in C[-1/2, 1/2] : -1 + \epsilon < u(x) \leq 0\}$$

*for any $\lambda \in [0, \lambda(\epsilon)]$.*

**Proof**. See [19].

By combining the result of Lemma 4.1 with Theorem 4.2 we obtain the following corollary.

COROLLARY 4.1. *For any $\epsilon > 0$, there exists a $\beta(\epsilon) > 0$ such that a unique solution to problem (NLP) may be found in the set $S_\epsilon$ for all $\beta \in [0, \beta(\epsilon)]$.*

**Proof (computer-assisted)**. Since the solution set $u(x, \lambda)$ to problem (LP) depends continuously on $\lambda$, we have that $\beta$ is a continuous function of $\lambda$ when defined by the mapping in Lemma 4.1. Further, $\beta(0) = 0$ and $\beta(\lambda(\epsilon)) > 0$ since the integral in problem (NLP) is finite. Hence solutions $u(x, \lambda)$ on $[0, \lambda(\epsilon)]$ are mapped continuously to solutions $u(x, \beta)$ on $[0, \beta(\epsilon)]$ for some $\beta(\epsilon)$ and we have an existence result. To obtain uniqueness, we rely upon a graphical argument. Uniqueness would imply that the mapping between $\lambda$ and $\beta$ is one-to-one. Over the entire space of solutions, this is not true. Rather, for $\chi > 0$, the mapping appears as in Figure 7. However, restricting attention to $S_\epsilon$ selects only part of the lower branch in Figure 7 and uniqueness results.

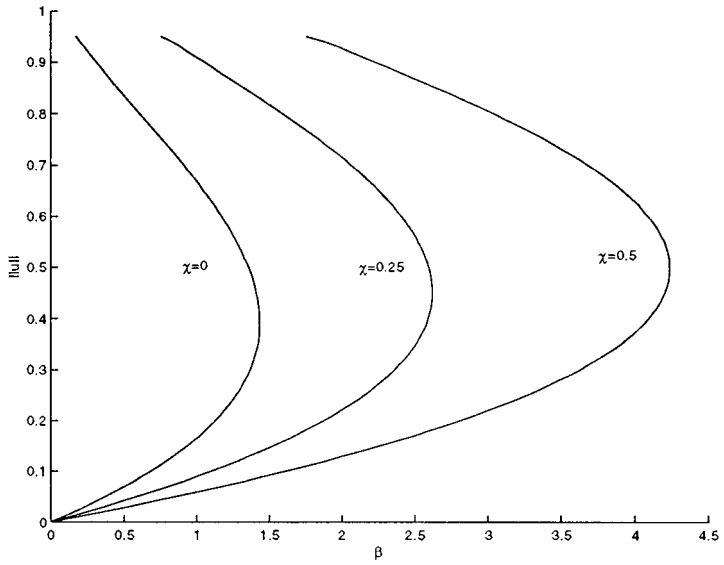


*Figure 8.* Bifurcation diagram for varactor capacitive control. The norm on $u$ is the maximum norm. Note that our analysis implies that the upper branch of each curve continues and tends towards a limiting singular solution at the point (0, 1).

The relationship between (NLP) and (LP) expressed in Lemma 4.1 is particularly useful when we wish to sketch the bifurcation diagram for (NLP). In [19] the following implicit formula's for the solution of problem (LP) were derived

$$\sqrt{\frac{(u+1)(u+1-\lambda/E)}{2E}} + \frac{\lambda}{E\sqrt{2E}} \tanh^{-1} \sqrt{\frac{u+1-\beta/E}{u+1}} = x, \tag{47}$$

$$\sqrt{\frac{1-\lambda/E}{2E}} + \frac{\lambda}{E\sqrt{2E}} \tanh^{-1} \sqrt{1-\lambda/E} = \frac{1}{2}. \tag{48}$$

By numerically solving Equation (48) for $E$ as a function of $\lambda$, using this result in Equation (47) to compute $u(x, \lambda)$, and combining with the mapping in Lemma 4.1, we may sketch the bifurcation diagram for problem (NLP). This is done in Figure 8 for various values of $\chi$.

We notice that the bifurcation diagram consists of a single fold for all values of $\chi \geq 0$. The pull-in instability may be described in terms of this bifurcation diagram. For values of $\beta$ less than some critical value $\beta^*$ two solutions exist, while as $\beta^*$ is approached, these two solutions coalesce and disappear. Since for $\beta$ beyond $\beta^*$ no solution exists, we conclude that $\beta^*$ corresponds to the pull-in voltage, *i.e.* this is the voltage beyond which the membrane collapses onto the rigid plate.

At this point, the analysis of the capacitive control scheme for our device is essentially complete. However, the reliance on the exact solution to (LP) in order to establish the pull-in property and sketch the bifurcation diagram for (NLP) is somewhat unsatisfying. In particular, if we wished to change from our 'strip' geometry to any other shape device, we cannot expect to have an exact solution to the local problem available. With this in mind, we present a few results which begin to generalize our analysis from the strip geometry to an arbitrarily shaped device. We begin by establishing the fact that the pull-in property is a generic feature of a

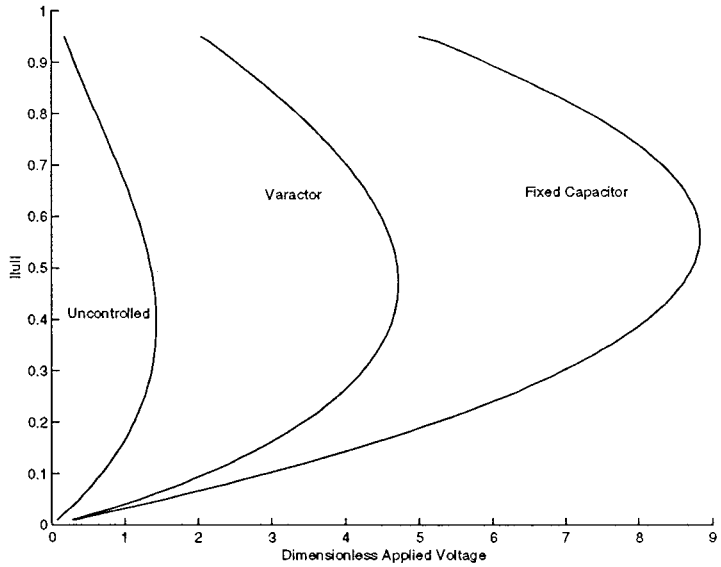


*Figure 9.* Bifurcation diagram for fixed capacitive control. The norm on $u$ is the maximum norm. Note that our analysis implies that the upper branch of each curve continues and tends towards a limiting singular solution at the point $(0, 1)$.

generalized local problem (GLP). That is, we show that the pull-in phenomena occurs for a MEMS device of rather arbitrary geometry.

THEOREM 4.4. *Let $\Omega$ be a bounded domain in $\Re^2$ with smooth boundary $\partial\Omega$. Consider*

$$-\triangle u = -\frac{\lambda}{(1+u)^2} \quad \text{on} \quad \Omega, \tag{49}$$

*with Dirichlet boundary condition*

$$u = 0 \quad \text{on} \quad \partial\Omega. \tag{50}$$

*Then, there exists a $\lambda^*$ such that no solution $u$ exists for any $\lambda > \lambda^*$.*

**Proof**. Let $\alpha_1$ be the lowest eigenvalue of

$$-\triangle u = \alpha u \quad \text{on} \quad \Omega, \tag{51}$$

$$u = 0 \quad \text{on} \quad \partial\Omega \tag{52}$$

with $v_1$ the associated eigenfunction. It is well known that $\alpha_1$ is simple and that $v_1$ may be chosen strictly positive in $\Omega$. Now, rewrite Equation (49) as

$$-\triangle u - \alpha_1 u = -\frac{\lambda}{(1+u)^2} - \alpha_1 u. \tag{53}$$

The solvability condition for this problem is then

$$\int_\Omega \left(\frac{\lambda}{(1+u)^2} + \alpha_1 u\right) v_1 = 0. \tag{54}$$

Since $v_1$ is strictly positive, the term in parenthesis must either be identically zero, or it must change sign. That it is not zero is clear. Hence, we are led to consider $\frac{\lambda}{(1+u)^2} + \alpha_1 u$. If this expression is to change sign, at some $u$, we must have $\frac{\lambda}{(1+u)^2} = -\alpha_1 u$. A simple plot of each side of this expression as a function of $u$ reveals that as $\lambda$ is increased beyond some value $\lambda^*$ the two curves no longer intersect and hence no solution exists for $\lambda > \lambda^*$.

We note that the proof is similar to the argument used to prove the existence of 'blow-up' in reaction diffusion systems or nonexistence in the Bratu problem, [27, pp. 652–654]. This similarity to problems arising in combustion or microwave heating suggests that techniques such as those found in [28] may be adapted to derive bounds on $\lambda^*$. Such an analysis is beyond the scope of this paper. Further, we again note that we have established that the pull-in phenomena occurs for an arbitrarily shaped planar electrostatically actuated MEMS device which is held fixed at the edges. Establishing that when embedded in the capacitive control scheme, an arbitrarily shaped device still possesses the pull-in property would require a detailed study of the mapping in Lemma 4.1 generalized as in Theorem 4.3 and examined for all possible shapes. We do not carry out such an analysis here. Rather, for our strip problem we demonstrate a methodology that allows one to determine if the controlled device still has the pull-in property, even when an exact solution to the local problem is unavailable.

The essential question is whether or not the curve of solutions in the bifurcation diagram 'bends back' upon itself. In Theorem 4.3, we proved that it does for (GLP) and from the exact solution in [19] we know that it does for (LP). Now, we must determine how this folded curve maps into the bifurcation diagram for (NLP) under the mapping in Lemma 4.1. To study this question, we map the solutions to the boundary value problem to the solutions of an initial-value problem. This technique which exploits the underlying symmetry in the equation, is well known in fluid dynamics. It is sometimes called exact shooting and was first introduced by Toepfer, [29], in 1912 in connection with the Blasius problem. In the 1960's and 1970's it was extended to a wide class of problems primarily through the work of Klamkin and Na. The interested reader is referred to Chapter 7 of [30] for a discussion and full list of references. We introduce the following initial-value problem (IVP)

$$\frac{\mathrm{d}^2 w}{\mathrm{d}x^2} = \frac{1}{w^2}, \tag{55}$$

$$w(0) = 1 \quad w'(0) = 0. \tag{56}$$

If we let $c = -u(0)$ then all solutions to (LP) can be generated from this initial-value problem by setting $u(x) = aw(bx) - 1$ and then requiring that

$$a = \frac{1}{w(b/2)}, \quad 1 - c = a, \quad \frac{\lambda}{a^3 b^2} = 1. \tag{57}$$

We may solve for $\lambda$ in terms of $b$ and $w$ to find that

$$\lambda = \frac{b^2}{w(b/2)^3}. \tag{58}$$

So, we see that the behavior of the bifurcation curve for (LP) may be obtained by studying solutions of (IVP) for $x \to \infty$. The asymptotic behavior of solutions to (IVP) for arbitrary initial conditions was presented in [19]. It was shown that

$$w(x) \sim \alpha x - \frac{1}{\alpha^2} \log(x) + \cdots. \tag{59}$$

Combining this with our expression for $\lambda$, we find that

$$\lambda \sim \frac{1}{\alpha b} \tag{60}$$

as $b \to \infty$. Hence as expected the bifurcation curve for (LP) bends back and approaches $\lambda = 0$. Finally, we may substitute our expressions for $\lambda$ and $u$ into our mapping in Lemma 4.1. We find that

$$\beta = \frac{b^2}{w(b/2)^3}\left(1 + \chi \frac{w(b/2)}{b}\int_{-b/2}^{b/2} \frac{dy}{w(y)}\right)^2. \tag{61}$$

Now, from our asymptotic approximation for $w$, we see that the first term in this expression goes like $1/b$ as $b \to \infty$ while the term in parentheses goes no faster than $\log(b)$. Hence the bifurcation curve for (NLP) also bends back and approaches $\beta = 0$. That is, the controlled device still possesses the pull-in property. Again note, only the asymptotic behavior of (IVP) was needed to obtain this result.

## 5. Analysis of varactor capacitive control

In this section we bring together our circuit analysis, approximate potential, and approximate capacitance calculations in order to derive a simple model of the elastic behavior of our MEMS device embedded in the varactor control circuit; see Figure 2.

First, making the small aspect ratio approximation, as was done in our field calculations, we may reduce our elastic model to

$$\frac{\mathrm{d}^2 u}{\mathrm{d}x^2} = \beta\left(\frac{\partial \psi}{\partial z}\right)^2, \tag{62}$$

$$u(-1/2) = u(1/2) = 0. \tag{63}$$

Now, recall from Section 3.1 that our approximate potential is given by

$$\psi = \frac{f(u)(1+z)}{1+u}. \tag{64}$$

We may use Equation (64) in Equation (62) to obtain

$$\frac{\mathrm{d}^2 u}{dx^2} = \frac{\beta f(u)^2}{(1+u)^2}, \tag{65}$$

$$u(-1/2) = u(1/2) = 0 \tag{66}$$

as the governing equations for the elastic displacement of our device when embedded in the varactor control circuit; see Figure 2.

For this varactor circuit, the specification of $f(u)$ is not as straightforward as it was for the fixed capacitor circuit. Recall that from Section 2.2 $f(u)$ is given by

$$f(u) = \frac{1}{1 + C/C_f}, \tag{67}$$

while the approximate normalized capacitance was given in Section 3.1 as

$$\frac{C}{C_0} = \int_{-1/2}^{1/2} \frac{\mathrm{d}\zeta}{1+u(\zeta)}. \tag{68}$$

Further recall that $C_f$ is not constant, but rather is defined by

$$C_f = C_m \left( \frac{1}{1 - V_f/V_0} \right)^{1/2}. \tag{69}$$

This expression for $C_f$ contains $V_f$ which is not known, but may be eliminated in favor of $V$ and $V_s$ through

$$V_f = -V - V_s. \tag{70}$$

While $V_s$ is specified, $V$ is unknown but must satisfy

$$V = \frac{-V_s}{1 + C/C_f}. \tag{71}$$

Taken together, Equations (65)–(71) complete the specification of our model for the elastic displacement of our device when embedded in the varactor control circuit.

We note that the analysis of this model will be more complicated than that for the simple capacitive control circuit. Nevertheless, the two models have much in common and our methods in the previous section suggest an approach here. First, we observe that this system, Equations (65)–(71), may still be viewed as a nonlocal and nonlinear elliptic problem. In particular, $f(u)$, while defined implicitly, is still simply a functional of $u$, with its dependence on $u$ given by Equation (68). Hence, we may still relate solutions of this problem to those of an associated local problem, (LP). Once again, the associated local problem is given by

$$\frac{\mathrm{d}^2 u}{\mathrm{d}x^2} = \frac{\lambda}{(1+u)^2}, \tag{72}$$

$$u(-1/2) = u(1/2) = 0 \tag{73}$$

and the relationship between solutions to our nonlocal varactor problem, (NVP), and this local problem, (LP), is summarized in the following lemma.

LEMMA 5.1. *A solution, $u$, of problem (NVP) is a solution of problem (LP) for $\lambda = \beta f^2(u)$ while a solution, $u$, of problem (LP) is a solution of problem (NVP) for $\beta = \frac{\lambda}{f^2(u)}$.*

**Proof**. Obvious.

Again, as in the previous section it is possible to use Lemma 5.1 to prove several results about the nature of solutions to (NVP). Since the algebra is tedious and the results similar to those in Section 4, we spare the reader this analysis. Rather, we use (LP) and Lemma 5.1 to sketch the bifurcation diagram for (NVP). This is done in Figure 9. The implications of these results are discussed in the following section.

## 6. Discussion

We began by formulating a model of an idealized electrostatically actuated MEMS device embedded in a control circuit. The model consisted of three parts. First, the electrostatic

potential on and around the device was assumed to satisfy Laplace's equation with the appropriate boundary conditions. Second, the elastic displacement of the device was assumed to satisfy an elliptic ordinary differential equation. The model geometry, a rectangular elastic membrane suspended above a rigid plate, together with assumptions concerning the elastic boundary conditions allowed us to make the assumption that the elastic displacement, $u$, was a function of a single spatial variable. We note that the electrostatic and elastic problems were coupled nonlinearly. That is, the location of the boundary conditions for the electrostatic problem depended upon the elastic displacement, while the forcing term in the elastic equation was proportional to the norm of the gradient of the potential, squared. The third part of the model consisted of equations governing the behavior of the circuit in which our MEMS device was embedded. These equations were derived by applying Kirchoff's laws. We note that the circuit equations were coupled to both the electrostatic and elastic problems. In particular, the potential drop specified in the electrostatic boundary conditions depended upon circuit behavior, while the circuit behavior depended upon the capacitance of the MEMS device and hence depended upon the elastic displacement, $u$.

Our next step was to simplify the model. Our main approximation was to use the small aspect ratio of our MEMS device to obtain an approximate solution to the potential equation. In engineering terms, we ignored fringing fields. The accuracy of this approximation was investigated in Subsection 3.2 by comparing the approximate solution to numerically obtained exact solutions. The upshot of this comparison is that for small aspect ratios, the approximate potential is very close to the exact. With this approximate solution in hand, we next turned to the elastic and circuit equations.

The reduced model, *i.e.* using the approximate potential, was studied for two different proposed control circuits. In order to see the effect of each control circuit it is useful to examine the behavior of our MEMS device when it is placed in a closed circuit with a fixed voltage source. We note that this corresponds to setting $\chi = 0$ in problem (NLP) from Section 4. As mentioned previously, this system was studied in [19]. The bifurcation diagram for positive values of $\beta$ is sketched in Figure 9 and corresponds to the $\chi = 0$ curve. We see that the bifurcation diagram consists of a single fold and hence for positive values of $\beta$ less than some critical value $\beta^*$, two solutions exist. As $\beta$ approaches $\beta^*$ these solutions collide and at $\beta^*$ they disappear. This critical value $\beta^*$ corresponds to the pull-in voltage and hence we have characterized the pull-in instability in terms of this bifurcation diagram. That is, for $\beta > \beta^*$, no steady-state solution of the problem exists, *i.e.* the elastic membrane has collapsed onto the rigid plate. We further note that under the assumption that the lower branch of the bifurcation diagram is the stable branch, the pull-in distance (maximum achievable displacement) corresponds to the value of $||u||$ at $\beta = \beta^*$. Observe that this distance is less than $1/2$.

Now, we can use our model to examine the effect of a control circuit on the stability of our MEMS device. We first turn our attention to the simple fixed capacitive control scheme proposed by Seeger and Crary in [4]. Seeger and Crary studied this scheme by using a simple mass-spring model to model the elastic behavior of a MEMS device. Further they concluded that the fixed capacitive control scheme fully stabilized the device, effectively removing the pull-in instability. At odds with this conclusion was the result obtained by Chan and Dutton in [6]. Chan and Dutton, like Seeger and Crary, used a mass-spring model, but they began to include two dimensional effects in an ad-hoc manner. On the basis of this model they concluded that pull-in persists. By plotting the bifurcation diagram for the fixed capacitive control model studied in Section 4, we also conclude that pull-in persists. Again turning to Figure 9 and this time focusing on curves for $\chi > 0$, we see that the bifurcation diagram for

this system is still characterized in terms of a single fold. Again, this implies that for $\beta$ greater than some critical value $\beta^*$, no steady solutions exist and pull-in has occurred. We also note that as $\chi$ is increased, the 'nose' of the curve moves up and to the right. This implies that the fixed capacitive scheme is partially stabilizing. That is, the achievable maximum displacement has increased. Again examining Figure 9, we see that this stabilization comes at a price, higher voltages are needed to obtain a given displacement.

In Section 5, we used our model to examine the effect of the varactor capacitive control scheme also proposed by Seeger and Crary, [5]. Again we note that Seeger and Crary's analysis, using a mass-spring model, indicated that this scheme should be fully stabilizing. They also concluded that it would stabilize the device with a lower energy expenditure than the fixed capacitive scheme. In Figure 8, we plot the bifurcation diagram for our model of the varactor control scheme. Once again, we see that the bifurcation diagram consists of a single fold and hence the pull-in instability persists. As with fixed capacitive control however, the scheme is partially stabilizing. Again we notice the 'nose' of the curve has moved up and to the right relative to the no control case. The maximum achievable displacement has increased. We also notice that Seeger and Crary's claim that the scheme requires a lower energy expenditure is correct. This is seen by noticing that the varactor curve lies in between the no control and fixed capacitive control curves in Figure 8. So, to get to a given displacement, the varactor scheme requires a smaller voltage than the fixed capacitive scheme.

Finally, we conclude with a few observations and open questions. We remind the reader that in Theorem 4.4 it was shown that the pull-in phenomena persists for an arbitrarily shaped planar MEMS device placed in a closed circuit with a fixed voltage source. The validity of this conclusion of course is limited to MEMS devices of small aspect ratio which may also be treated as elastic membranes. While we did not examine the effect of capacitive control schemes on arbitrarily shaped devices, we introduced an approach in Section 4 that should prove useful for carrying out such an analysis. That is, while we cannot convert a 2-D boundary value problem to an initial value problem, the symmetries present in 1-D persist in 2-D and may be exploited. The authors are currently attempting such an analysis and invite the interested reader to further ponder the effect of shape on the behavior of electrostatically actuated MEMS devices.

## Acknowledgements

The author's thank all of the referees for their careful reading of the paper and numerous useful comments.

## References

1. W.S.N. Trimmer, Microrobots and micromechanical systems. *Sens. Actuat.* 19 (1989) 267–287.
2. H.C. Nathanson, W.E. Newell, R.A. Wickstrom and J.R. Davis, The resonant gate transistor. *IEEE Trans. on Electron Devices* 14 (1967) 117–133.
3. P.B. Chu and K.S.J. Pister, Analysis of closed-loop control of parallel-plate electrostatic microgrippers. *Proc. IEEE Int. Conf. Robotics and Automation* (1994) pp. 820–825.
4. J.I. Seeger and S.B. Crary, Stabilization of electrostatically actuated mechanical devices. *Proceedings of the 1997 International Conference on Solid-State Sensors and Actuators* (1997) pp. 1133–1136.
5. J.J. Seeger and S.B. Crary, Analysis and simulation of MOS capacitor feedback for stabilizing electrostatically actuated mechanical devices. *Second Int. Conf. on the Simulation and Design of Microsystems and Microstructures – MICROSIM97* (1997) pp. 199–208.

6. E.K. Chan and R.W. Dutton, Effects of capacitors, resistors and residual change on the static and dynamic performance of electrostatically actuated devices. *Proc. SPIE* 3680 (1999) 120–130.
7. H.A.C. Tilmans and R. Legtenberg, Electrostatically driven vacuum-encapsulated polysilicon resonators. Part II. theory and performance. *Sens. Actuat. A* 45 (1994) 67–84.
8. C.H. Mastrangelo and C.H. Hsu, Mechanical stability and adhesion of microstructures under capillary forces – Part I: Basic theory. *J. Microelectromech. Syst.* 2 (1993) 33–??.
9. J.R. Gilbert, G.K. Ananthasuresh, and S.D. Senturia, 3D modeling of contact problems and hysteresis in coupled electro-mechanics. *Proceedings of the 9th Annual International Workshop on Micro Electro Mechanical Systems* (1996) pp. 127–132.
10. M.T.A. Saif, B.E. Alaca and H. Sehitoglu, Analytical modeling of electrostatic membrane actuator micro pumps. *IEEE J. Microelectromech. Syst.* 8 (1999) 335–344.
11. O. Francais and I. Dufour, Enhancement of elementary displaced volume with electrostatically actuated diaphragms: application to electrostatic micropumps *J. Micromech. Microeng.* 10 (2000) 282–286.
12. R. Apte, F. Sandejas, W. Banyai and D. Bloom, Grating light valves for high resolution displays. *Solid State Sensors and Actuators Workshop* June (1994) pp. ???–???.
13. S. Timoshenko, *Theory of Plates and Shells*. New York: McGraw-Hill Book Company (1940) 492 pp.
14. A. Dec and K. Suyama, Micromachined varactor with wide tuning range. *Electron. Lett.* 33 (1997) 22–25.
15. O. Francais and I. Dufour, Dynamic simulation of an electrostatic micropump with pull-in and hysteresis phenomena. *Sens. Actuat. A* 70 (1998) 56–60.
16. N. Tas, J. Wissink, L. Sander, T. Lammerink and M. Elwenspoek, Modeling, design and testing of an electrostatic shuffle motor. *Sens. Actuat. A* 70 (1998) 171–178.
17. C. Hsu and W. Hsu, A two-way membrane-type micro-actuator with continuous deflections. *J. Micromech. Microeng.* 10 (2000) 387–394.
18. J.R. Gilbert and S.D. Senturia, Two-phase actuators: stable zipping devices without fabrication of curved structures. *Solid-State Sensor and Actuator Workshop* (1996) pp. 98–100.
19. D. Bernstein, P. Guidotti and J.A. Pelesko, Analytical and numerical analysis of electrostatically actuated mems devices. *Proceeding of Modeling and Simulation of Microsystems 2000* (2000) pp. 489–492.
20. P. Penfield Jr. and R.P. Rafuse, *Varactor Applications*. Cambridge: MIT Press (1962) 623pp.
21. A.N. Semakhin and G.A. Shneerson, calculation of the leading corrections to the 'capacitor' capacitance between two conductors separated by a small gap. *Sov. Phys. Tech. Phys.* 35 (1990) 1115–1119.
22. M.R. Boyd, S.B. Crary and M.D. Giles, A heuristic approach to the electromechanical modeling of MEMS beams. *Technical Digest Solid-State Sensor and Actuator Workshop* (1994) pp. 123–126.
23. R.F. Harrington, *Field Computation by Moment Methods*. Piscataway, NJ: IEEE Press (1993) 229 pp.
24. A.A. Lacey, Thermal runaway in a non-local problem modelling ohmic heating: Part I: model derivation and some special cases. *Eur. J. Appl. Math.* 6 (1995) 127–144.
25. A.A. Lacey, thermal runaway in a non-local problem modelling ohmic heating: Part II: general proof of blow-up and asymptotics of runaway. *Eur. J. Appl. Math.* 6 (1995) 201–224.
26. J.A. Carrillo, On a nonlocal elliptic equation with decreasing nonlinearity arising in plasma physics and heat conduction. *Nonlin. Anal. Meth. Applic.* 32 (1998) 97–115.
27. I. Stakgold, *Green's Functions and Boundary Value Problems*. New York: Wiley (1998) 689 pp.
28. J. Bebernes and D. Eberly, *Mathematical Problems from Combustion Theory*. New York: Springer-Verlag (1989) 177 pp.
29. K. Toepfer, Grenzschichten in flussigkeiten mit kleiner reibung. *Z. Math. Phys.* 60 (1912) 397–398.
30. T.Y. Na, *Computational Methods in Engineering Boundary Value Problems*. New York: Academic Press (1979) 309 pp.